Functional QSM at 9.4T with single echo gradient-echo and EPI acquisition

Dávid Balla, Philipp Ehses, Rolf Pohmann, Juliane Budde, Christian Mirkes, G. Shajan, Klaus Scheffler*
High-field MR Centre
Max Planck Institute for Biological Cybernetics
Tübingen, Germany
**david.balla@tuebingen.mpg.de*

Philipp Ehses, Christian Mirkes, Klaus Scheffler
Department of Biomedical Magnetic Resonance
University of Tübingen
Tübingen, Germany

Richard Bowtell
Sir Peter Mansfield Magnetic Resonance Centre
University of Nottingham
Nottingham, Great Britain

***Abstract*—Functional quantitative susceptibility mapping was performed on high resolution time-series acquired at 9.4T. Two alternative pulse sequences, two functional stimulation paradigms and three susceptibility mapping pipelines were evaluated. In addition to the conventional statistical parametric mapping of brain activation, also multivariate processing was performed in order to investigate the effect of physiological variations on the signal, and to learn about possible differences between these effects in the evolution of signal modulus and the evolution of calculated susceptibilities. The results provide useful information on the potential and the technical limitations of functional quantitative susceptibility mapping at 9.4T.**

Keywords—fQSM; BOLD; phase fMRI; 9.4T; dynamic susceptibility changes

I. INTRODUCTION

The contrast in gradient echo (GE) BOLD fMRI depends on the underlying susceptibility changes in a non-linear manner. Quantitative measurement of brain activation related susceptibility changes requires dynamic T2*-mapping sequences. Functional QSM (fQSM) was proposed as an alternative method [1], which calculates susceptibility changes directly from a complex GE-fMRI time-series. The advantages of fQSM relative to dynamic T2*-mapping are:

- fQSM does not require the acquisition of time-series with a special pulse sequence. fMRI and fQSM activation maps can be calculated from the same time-series.
- fQSM maps susceptibility changes, not their effects (e.g. T2* changes).
- fQSM deconvolves non-local field effects, resulting in activation maps with a high neural tissue specificity.

fQSM was recently applied for the analysis of GE BOLD contrast in zoomed EPI time-series acquired at 7T [2]. The comparison of fQSM and fMRI activation maps, which were calculated using a general linear model (GLM) fit with an arbitrary threshold, revealed some issues calling for clarification. The main limitation of fQSM in its current form is the high number of statistically significant voxels, which are not coincidentally significant in fMRI maps ("uncommon voxels").

Here we exploit time-series obtained at 9.4T with full brain coverage GE-EPI and single echo "shifted" gradient-echo (esGRE) [3] for fMRI and fQSM analysis. In addition to the GLM fit, we additionally use multivariate processing of modulus and susceptibility time-series in order to identify spectral components of contrast variance.

II. METHODS

A. Experiments

Experiments were performed on a 9.4T system equipped with a custom-built 16-channel transmit-coil and a 31-channel receive-array helmet [4]. The visual stimulus for fMRI consisted of a flickering checkerboard disk stimulus on a grey background. The motor-task was tapping of the thumbs of both hands with the four other fingers in quick cyclic runs. Both paradigms are expected to produce positive BOLD contrast in respective cortical areas in the magnitude time-series.

B. Acquisition strategies

- Slice interleaved esGRE sequence [3] providing distortion-free T2*-weighted images with TE=17.5ms and TR=112ms (2 echo shifts); further parameters were: 1mm isotropic resolution, volume TR_{visual}=5.04s, TR_{motor}=5.38s, 100 repetitions and 3-fold acceleration. Combining echo-shifting with slice interleaving allows a prolonged TR *and* TE without a significant scan time increase [5]. Furthermore, slice interleaved esGRE does not show the additional signal loss that is usually associated with echo-shifted sequences, since only a single RF pulse is applied per slice and TR (illustrated

in Fig. 1). Thus, the signal equation for slice interleaved esGRE is identical to that of a conventional spoiled GRE.

- GE-EPI with 1mm isotropic resolution, TE/TR = 24ms/3s, 100 repetitions and 4-fold acceleration.

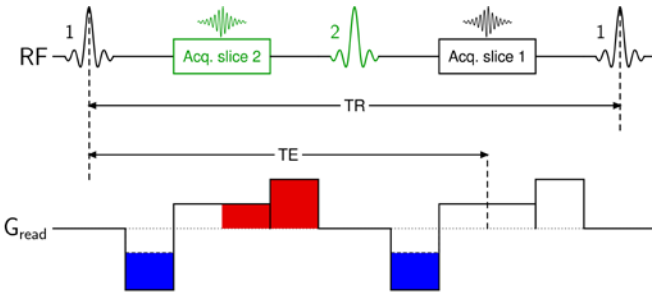

Figure 1: Interleaved esGRE pulse sequence diagram

C. Processing

- SDI (Superfast dipole inversion) [6] was applied with σ=0.016 and δ=2/3.

- Homodyne-MEDI: Two dimensional Gaussian high-pass filtering of the phase with 6mm filter width was performed, followed by an iterative dipole deconvolution with regularization using edge information derived from the modulus images as a priori knowledge (MEDI) [7,8]. Iteration steps were limited to 15 to avoid overfitting. The noise threshold was 16.

- SHARP-MEDI: The phase was unwrapped [9], followed by the application of the SHARP method [10] with a r=2mm spherical kernel and the threshold parameter set to 0.1 for the removal of phase components from sources outside the brain. QSMs were subsequently calculated using MEDI.

- pICA: Multivariate processing was performed using probabilistic independent component analysis (pICA) [11] with the MELODIC tool in FSL. Timecourses were variance-normalized and the number of calculated independent components (IC) was limited to 30 in order to avoid overfitting and to save processing time. Only QSM-series calculated with SDI were analyzed with pICA.

- FEAT: Single variable processing was performed with the FEAT tool in FSL. The preprocessing consisted of motion correction with MCFLIRT [12], temporal high-pass filtering and pre-whitening. All QSM-series were analyzed with FEAT.

III. Results

Figure 2 presents QSMs acquired and reconstructed with different techniques. High resolution anatomical maps acquired in 7 min and reconstructed using SHARP with a kernel radius r=6mm and a threshold set to 0.2, followed by MEDI, demonstrate the efficiency of performing QSM at 9.4T. For QSM-series intended to be used for fQSM, radii of SHARP kernels were kept as short as possible in order to avoid cropping of cortical voxels close to the surface of the brain. As expected, QSMs calculated with SDI involving threshold based k-space division (TKD) [13,14] have a higher noise level than maps calculated with regularized inversion. However, at the positions pointed out by arrows, MEDI, in contrast to SDI, did not yield the expected positive contrast in the cortex.

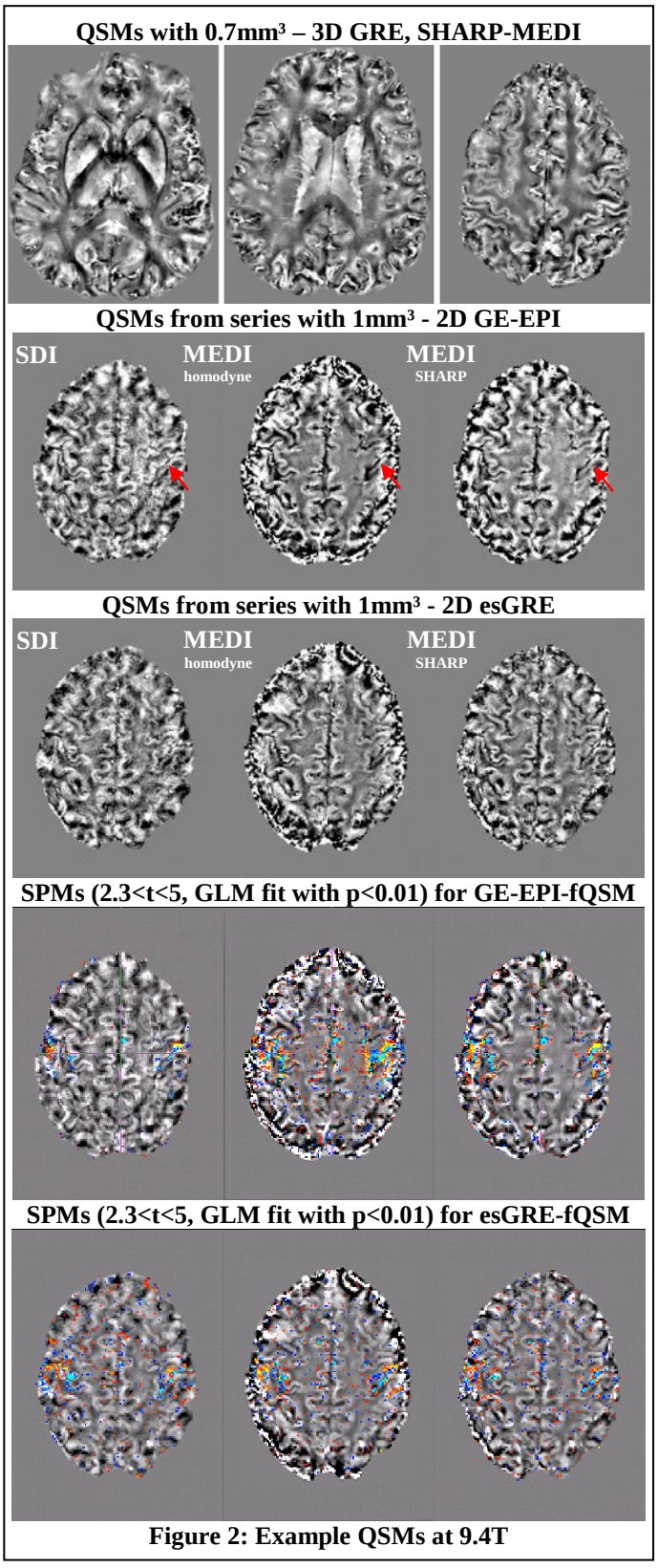

Figure 2: Example QSMs at 9.4T

Figure 2 also presents the fQSM activation maps related to the three alternative processing approaches. For GE-EPI homodyne-MEDI works efficiently, presumably because homodyne high-pass filtering reduces the temporal variance of physiological origin within the brain. In contrast, SHARP and SDI only affect the phase modulation generated by external sources. For esGRE, which is less sensitive to physiological noise than GE-EPI, the three methods provide very similar activation maps. The conventional fMRI SPMs for the same dataset are presented in the first column of Fig. 3. There is a good qualitative correspondence between fMRI and fQSM SPMs in case of the experiments with motoric activation. However, the FEAT results for the QSM-series calculated from the datasets acquired during the visual stimulation paradigm are not comparable to the modulus SPMs (Fig. 3 second and third column). Summing up the independent spectral components identified with pICA resulted in the maps presented in the fourth column of Fig. 3.

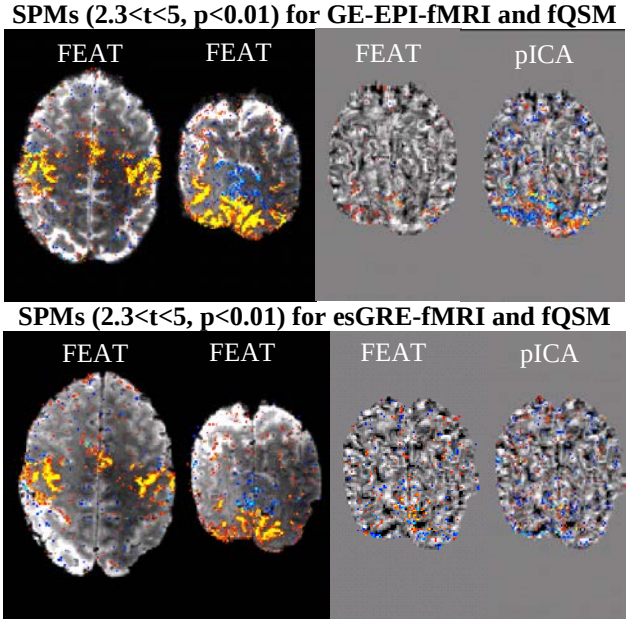

Figure 4: Motor and visual SPMs

Figure 4 demonstrates some features of the pICA for the visual GE-EPI modulus and QSM-series and illustrates the ICs related to brain activation, motion and breathing. IC11 in the modulus decomposition was tentatively assigned to variance introduced by breathing. A similar modulation is already detected as IC2 for the QSM-series. In contrast, activation related periodic modulation is IC5 in fMRI and only IC16 in fQSM. Thresholded IC-maps in Fig. 4 demonstrate the effect of individual spectral components. The effects of motion and brain activation are similar in fMRI and fQSM and, hence, only the effect of breathing in combination with interleaved slice sampling is shown explicitly in case of fQSM.

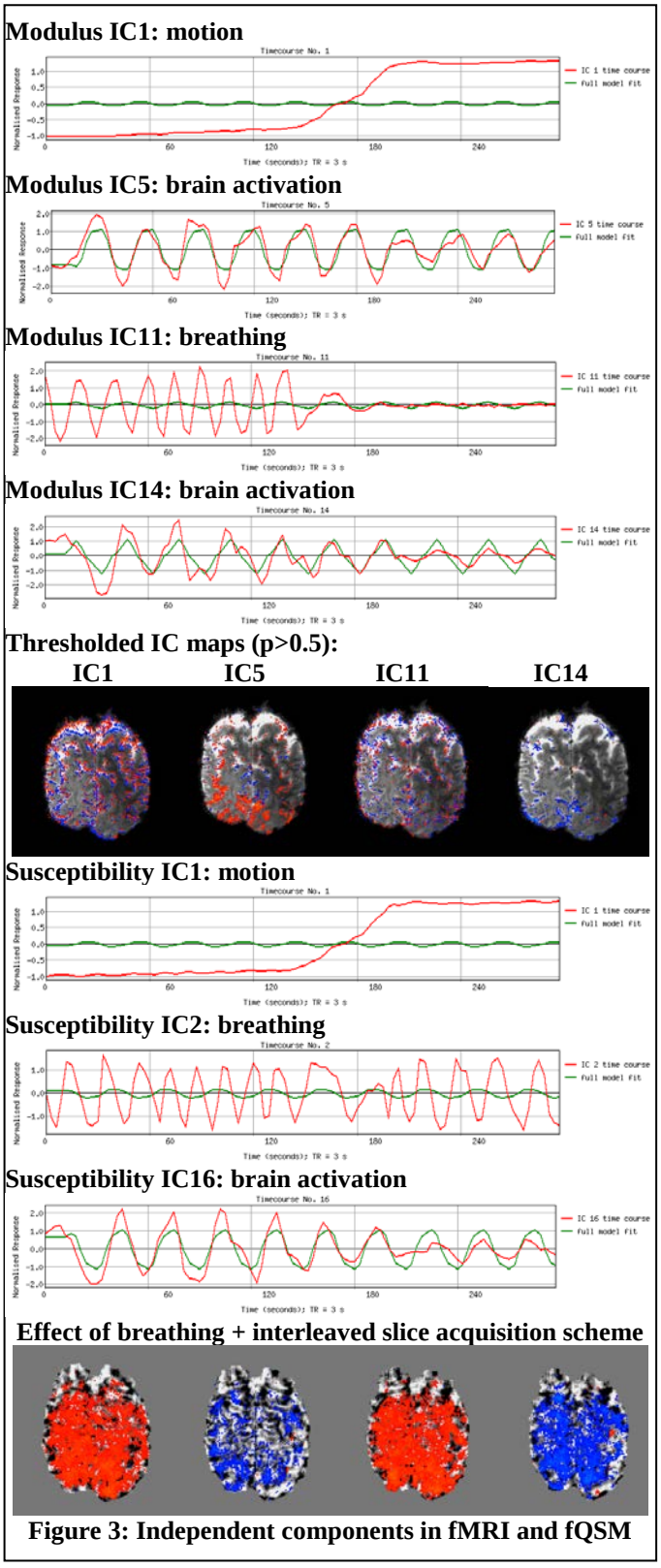

Figure 3: Independent components in fMRI and fQSM

IV. Conclusion

The presented results demonstrate the feasibility of fQSM at 9.4T. Slice interleaved esGRE acquisition is a useful alternative to GE-EPI especially, if distortions are critical. The SDI approach proved to be very efficient for calculating QSM-series for fQSM. However, temporal filtering may be necessary in combination with SDI for optimal quality of fQSMs. Multivariate processing was successful in identifying spectral components in the modulus and susceptibility evolution related to motion, breathing as well as separating activation related changes from confounding effects. Further work needs to address the optimization of the fQSM pipeline based on multivariate processing.

References

[1] D. Z. Balla, R. M. Sanchez-Panchuelo, S. Wharton, G. E. Hagberg, K. Scheffler, S. Francis, R. Bowtell, "Functional Quantitative Susceptibility Mapping (fQSM)", Proceedings of the ISMRM, Melbourne, Australia, 2012, program number 325.

[2] D. Z. Balla, R. M. Sanchez-Panchuelo, S. Wharton, G. E. Hagberg, K. Scheffler, S. Francis, R. Bowtell, "Experimental investigation of the relation between gradient echo BOLD fMRI contrast and underlying susceptibility changes at 7T", Proceedings of the ISMRM, Salt Lake City, USA, 2013, program number 300.

[3] P. Ehses, J. Budde, G. Shajan, K. Scheffler, "Distortion-free high-resolution fMRI at 9.4T", Proceedings of the ISMRM, Melbourne, Australia, 2012, program number 329.

[4] G. Shajan, M. Kozlov, J. Hoffmann, R. Turner, K. Scheffler, R. Pohmann, "A 16-channel dual-row transmit array in combination with a 31-element receive array for human brain imaging at 9.4T", MRM, in press.

[5] Andrew Gibson, Andrew M. Peters, Richard Bowtell, Echo-shifted multislice EPI for high-speed fMRI, Magnetic Resonance Imaging, Volume 24, Issue 4, May 2006, Pages 433-442, ISSN 0730-725X, 10.1016/j.mri.2005.12.030.

[6] F. Schweser, A. Deistung, K. Sommer, J. R. Reichenbach, "Toward online reconstruction of quantitative susceptbility maps: Superfast dipole inversion", MRM 69(6):1581-1593, 2013

[7] Wharton SJ, Bowtell R. Whole-brain susceptibility mapping at high field: a comparison of multiple- and single-orientation methods. NeuroImage 2010*;* 53*:* 515–525.

[8] Liu T, Liu J, de Rochefort L, Spincemaille P, Khalidov I, Ledoux JR, Wang Y. Morphology enabled dipole inversion (MEDI) from a single-angle acquisition: comparison with COSMOS in human brain imaging. Magn Reson Med 2011*;* 66*:* 777–783.

[9] Schofield MA, Zhu Y. Fast phase unwrapping algorithm for interferometric applications. Opt Lett 2003*;* 28*:* 1194–1196.

[10] Schweser F, Deistung A, Lehr BW, Reichenbach JR. Quantitative imaging of intrinsic magnetic tissue properties using MRI signal phase: an approach to in vivo brain iron metabolism? NeuroImage 2011*;* 54*:* 2789–2807.

[11] Beckmann, C.F.; Smith, S.M., "Probabilistic independent component analysis for functional magnetic resonance imaging," Medical Imaging, IEEE Transactions on , vol.23, no.2, pp.137,152, Feb. 2004

[12] Jenkinson, M., Bannister, P., Brady, M., & Smith, S. (2002). Improved optimization for the robust and accurate linear registration and motion correction of brain images. Neuroimage, 17(2), 825-841.

[13] Shmueli K, de wart JA, van Gelderen P, Li TQ, Dodd SJ, Duyn JH. Magnetic susceptibility mapping of brain tissue in vivo using MRI phase data. Magn Reson Med 2009*;* 62*:* 1510–1522.

[14] Wharton, S., Schäfer, A., & Bowtell, R. (2010). Susceptibility mapping in the human brain using threshold-based k-space division. Magnetic Resonance in Medicine, 63(5), 1292-1304.